# Quasielastic charged-current neutrino-nucleus scattering with relativistic nuclear models

K. S. Kim,[1,*] Soonchul Choi,[2] Tsuyoshi Miyatsu,[3] Myung-Ki Cheoun,[3] Hungchong Kim,[4] and W. Y. So[5]

[1]*School of Liberal Arts and Science, Korea Aerospace University, Goyang 10540, Korea*
[2]*Center for Exotic Nuclear Studies, Institute for Basic Science, Daejeon 34126, Korea*
[3]*Department of Physics and OMEG Institute, Soongsil University, Seoul 06978, Korea*
[4]*Center for Extreme Nuclear Matters, Korea University, Seoul 02841, Korea*
[5]*Department of Radiological Science, Kangwon National University at Dogye, Samcheok 25945, Korea*

(Received 22 September 2022; revised 14 December 2022; accepted 2 February 2023; published 14 February 2023)

Charged-current neutrino-nucleus scattering is studied in the quasielastic region with various relativistic nuclear models that include the relativistic Hartree, the nonlinear $\sigma$, the quark-meson coupling, and the chiral quark-meson coupling models. Theoretical results at several kinematics are compared with experimental data measured from MiniBooNE, T2K, MicroBooNE, and SciBooNE. While the theoretical double-differential cross sections in terms of the kinetic energy and polar angle of outgoing muon describe the T2K data well, the single-differential cross sections in terms of energy loss and the total cross sections of incident neutrino energy do not properly describe MiniBooNE, MicroBooNE, and SciBooNE data. Additionally, differences from the relativistic nuclear models are examined in detail by comparing with the experimental data. In particular, the MiniBooNE data are not consistent with MicroBooNE and SciBooNE data, where the incident neutrino energies are below 1 GeV.

DOI: 10.1103/PhysRevC.107.024607

## I. INTRODUCTION

In the last decade, the cross sections of neutrino-nucleus ($\nu$-$A$) scattering have been measured at NOMAD [1], MiniBooNE [2–6], SciBooNE [7,8], MINER$\nu$A [9], MINOS [10], T2K [11,12], NO$\nu$A [13], and MicroBooNE [14,15]. These experiments have improved the accuracy for the measurements of differential cross sections from various target nuclei. The main goal of these experiments is to provide clues for unsolved problems such as the neutrino mass, neutrino oscillation, Dirac or Majorana particle, and so on.

Quasielastic $\nu$-$A$ scattering is one of tools to study not only neutrino puzzles but also properties of target nucleus. Because the energy of the incident neutrino can hardly be fixed, its energy flux is taken by averaging the incident energy. In particular, this interaction requires accurate information of neutrino kinematics, target nucleus, and electroweak current operator. The relativistic mean-field (RMF) model [16], the random-phase approximation (RPA) [17], the Fermi gas model [18], and so on [19] are mainly used as the nuclear model to describe the quasielastic scattering. The electroweak current operator is consisted of two vectors, one axial vector, and one pseudoscalar form factors.

For the inclusive charged-current (CC) quasielastic $\nu$-$A$ scattering, where the outgoing charged lepton is only measured, observable quantities are the angle and the kinetic energy of the final lepton. Because of the wide energy distribution of neutrino beam, it is difficult to determine the energy of the neutrino and subsequently it is crucial to identify the outgoing charged lepton. For the analysis, the neutrino energy $E_\nu^{QE}$ and squared four-momentum transfer $Q^2_{QE}$ are reconstructed in the CC quasielastic region [2]:

$$E_\nu^{QE} = \frac{2M'_n E_l - \left(M'^2_n + m_l^2 - M_p^2\right)}{2M'_n - 2E_l + 2\sqrt{E_l^2 - m_l^2}\cos\theta_l},$$

$$Q^2_{QE} = -m_l^2 + 2E_\nu^{QE}\left(E_l - \sqrt{E_l^2 - m_l^2}\cos\theta_l\right),$$

where $E_l = T_l + m_l$ is the total energy of the outgoing lepton with the kinetic energy of the lepton $T_l$, and $M_n$, $M_p$, $m_l$ are the neutron, proton, and outgoing lepton masses. $M'_n = M_n - E_b$ is the adjusted neutron mass depended on the binding energy $E_b$. The reconstructed energy $E_\nu^{QE}$ can be theoretically calculated straightforward but it is not good enough to estimate true neutrino energy due to dynamics of nucleons in target nucleus. We note that there are several papers to discuss the kinematics of nucleons in the quasielastic region [20–22].

Not only the neutrino kinematics but also the axial mass form factor and the strangeness contents on the nucleons turn out to be important ingredients. Through the CC reaction, in particular, the axial mass was measured with $M_A = 1.05 \pm 0.02(\text{stat}) \pm 0.06(\text{syst})$ GeV with $3 < E_\nu < 100$ GeV at NOMAD [1]. At MiniBooNE [2], the CC quasielastic double-differential cross sections ($\frac{d^2\sigma}{dT_\mu d\cos\theta_\mu}$), single-differential cross section ($\frac{d\sigma}{dQ^2}$), and flux-unfold cross sections were measured using muon neutrino interaction on $^{12}$C with the $0 < E_\nu < 3$ GeV region and the $M_A = 1.35 \pm 0.17$ GeV was extracted. Another experiment at MiniBooNE [3] measured the

*kyungsik@kau.ac.kr

 

differential cross section ($\frac{d\sigma}{dQ^2}$) on $CH_2$ for neutrino neutral-current (NC) reaction and the strange axial form factor was obtained $g_A^s = 0.08 \pm 0.26$ at squared four-momentum transfer $Q^2 = 0$. The antineutrino CC and NC reactions were measured at MiniBooNE [4,5]. Recently, a new CC cross section with monoenergetic muon neutrino at 236 MeV was measured from MiniBooNE [6], that the neutrinos are generated from the decay of kaon at rest, called kaon-decays-at rest (KDAR).

The muon neutrino CC inclusive cross sections were measured with both NEUT- and NUANCE-based simulations and both results are consistent with SciBooNE [7], and the analysis of combined MiniBooNE/SciBooNE data was performed for $\nu_\mu$ and $\bar{\nu}_\mu$ disappearance [8]. The value of $M_A = 0.99$ GeV for $\bar{\nu}_\mu$ CC reaction was obtained at MINER$\nu$A Collaboration [9] in the NuMI neutrino beam, which is in agreement with standard value, 1.032 GeV. The other value of $M_A = 1.23^{+0.13}_{-0.09}(\text{fit})^{+0.12}_{-0.15}(\text{syst})$ GeV was measured at MINOS [10] in quasielastic scattering of muon neutrino on $^{56}$Fe with the average energy $\langle E_\nu \rangle = 2.79$ GeV. The experiment of muon neutrino CC interaction was also performed without pion in the final state at T2K [11,12] and then $M_A$ was measured to be $1.26^{+0.21}_{-0.18}$ GeV. At NOvA [13], the first measurement of the oscillation of muon neutrino into electron neutrino was reported. New muon neutrino scattering for the CC reaction was performed on $^{40}$Ar at MicroBooNE and measured the cross sections for various kinematics [14,15]. Note that the values of $M_A$ are well summarized in Ref. [23].

There have been many theoretical works [24–32] for analyses of the CC quasielastic experiments. Within a relativistic distorted impulse approximation (RDWIA), the authors in Refs. [24,25] calculated the CC $\nu_\mu$-$^{12}$C and $\nu_\mu$-$^{40}$Ar quasielastic scattering and determined $1 \leqslant M_A \leqslant 1.20$ GeV in comparison with MiniBooNE and MicroBooNE data. In Ref. [27], the CC double-differential cross section was compared with the MiniBooNE data by including a many-body expansion of the gauge boson absorption. The experimental data from MiniBooNE, T2K, MINER$\nu$A, NOMAD, and SciBooNE were analyzed within the framework of extended superscaling approach (SUSAv2) by including the MEC and found that the contribution of the 2p-2h is about 15%–25% depending on the kinematics [29]. In Ref. [30], the effects of the strange axial form factor and axial mass were discussed for both NC and CC quasielastic interactions from $^{12}$C, $^{40}$Ca, $^{56}$Fe, and $^{208}$Pb within the quantum hadrodynamics (QHD) model and the role of $g_A^s$ is found to increase with heavier nuclei. The authors in Ref. [32] calculated the CC quasielastic scattering with nonrelativistic nuclear energy density functional and then the effect of isoscalar mass is dominated but that of isovector effective mass can be neglected.

The QHD, as a representative RMF nuclear model, has been established by Walecka within a relativistic framework for describing nuclear many-body system, where the point-like nucleons interact through the exchange of scalar ($\sigma$) and vector ($\omega$) meson [33]. This model has achieved great success in understanding the saturation mechanism of infinite matter and the characteristics of doubly magic nuclei with the inclusion of isovector ($\rho$) meson [34]. Boguta and Bodmer introduced a nonlinear $\sigma$ self-coupling, the so-called nonlinear $\sigma$ (NL) model [35], to reproduce the realistic nuclear incompressibility because the equation of state (EoS) given by the *naive* QHD was too hard. The NL has been used to describe not only light doubly magic nuclei but heavy deformed nuclei [36,37]. Guichon [38] propose the quark-meson coupling (QMC) model, in which the properties of nuclear matter can be self-consistently calculated by the coupling of meson fields to the *quarks* within the nucleons rather than to the nucleons themselves [39]. In addition, the QMC model has been extended to include quark-quark hyperfine interactions due to exchanges of gluon and pion based on chiral symmetry [40]. This new version of the chiral QMC (CQMC) model guarantees the conservation of axial vector current in chiral limit, and it was applied to the neutron-star EoS within relativistic Hartree-Fock approximation [41]. These models were recently applied into the exclusive $(e, e'p)$ [42] and inclusive $(e, e')$ [43] reactions for electron-nucleus quasielastic scattering and shown to be in good agreement with the experimental data. The detail explanations of each models are in Ref. [42].

In the present work, we calculate the muon neutrino CC interaction from $^{12}$C and $^{40}$Ar in the quasielastic region and compare the calculated various cross sections with MiniBooNE, T2K, SciBooNE, and MicroBooNE data. In these calculations, the wave functions of bound nucleons in target nucleus are generated from the QHD, NL, QMC, and CQMC models and the wave functions of the continuum nucleons are obtained by solving the Dirac equation with the scalar and vector potentials generated from the same models of the bound nucleons. This method guarantees current conservation and gauge invariance. In Refs. [44,45], the energy-dependent potential of the knocked-out nucleon was studied to include the large momentum transfer. In order to keep the current conservation and gauge invariance, the same potential is used in this work. For the Coulomb distortion of outgoing muon from target nucleus, the same approximation exploited by Ohio group [46] is used. Especially, the difference between these models is small on the exclusive $(e, e'p)$ reaction [42], but on the inclusive $(e, e')$ reaction [43], the difference is large because of summing all bound nucleons.

In the present paper, the formalism of the inclusive CC $\nu$-$A$ scattering is briefly introduced in Sec. II, and Sec. III presents the results and discussion. Finally, we summarize the work in Sec. IV.

## II. FORMALISM

In the quasielastic $\nu(\bar{\nu})$-$A$ scattering, we choose that the target nucleus is seated at the origin of the coordinate system. The four-momenta of the participating bodies are denoted as $p_i^\mu = (E_i, \mathbf{p}_i)$, $p_f^\mu = (E_f, \mathbf{p}_f)$, $p_A^\mu = (E_A, \mathbf{p}_A)$, $p_{A-1}^\mu = (E_{A-1}, \mathbf{p}_{A-1})$, and $p^\mu = (E_N, \mathbf{p})$ for the incident neutrino, outgoing muon, target nucleus, the residual nucleus, and the knocked-out nucleon, respectively. Within the laboratory frame, the inclusive cross section in the CC reaction, which detects only outgoing lepton, is given by the contraction

between lepton and hadron tensors:

$$\frac{d\sigma}{dT_N} = 4\pi^2 \frac{M_N M_{A-1}}{(2\pi)^3 M_A} \int \sin\theta_l d\theta_l \int \sin\theta_N d\theta_N p f_{\rm rec}^{-1} \sigma_M^{W^\pm} \times [v_L R_L + v_T R_T + h v'_T R'_T], \quad (1)$$

where $M_N$ is the nucleon mass in free space, $\theta_l$ denotes the scattering angle of the lepton, $\theta_N$ is the polar angle of knocked-out nucleons, $T_N$ is the kinetic energy of the knocked-out nucleon, and $h = -1$ ($h = +1$) corresponds to the intrinsic helicity of the incident neutrino (antineutrino). The $R_L, R_T$, and $R'_T$ are longitudinal, transverse, and transverse interference response functions, respectively. Detailed forms for the kinematical coefficients $v$ and the corresponding response functions $R$ are given in Ref. [16]. The squared four-momentum transfer is given by $Q^2 = q^2 - \omega^2 = -q_\mu^2$. For the CC reaction, the kinematic factor $\sigma_M^{W^\pm}$ is defined by

$$\sigma_M^{W^\pm} = \sqrt{1 - \frac{M_l^2}{E_f}} \left( \frac{G_F \cos(\theta_C) E_f M_W^2}{2\pi (Q^2 + M_W^2)} \right)^2, \quad (2)$$

where $M_W$ is the rest mass of the $W$ boson, and $M_l$ is the mass of an outgoing lepton. $\theta_C$ represents the Cabibbo angle given by $\cos^2\theta_C \simeq 0.9749$. $G_F$ denotes the Fermi constant. The recoil factor $f_{\rm rec}$ is written as

$$f_{\rm rec} = \frac{E_{A-1}}{M_A} \left| 1 + \frac{E_N}{E_{A-1}} \left[ 1 - \frac{\mathbf{q}\cdot\mathbf{p}}{p^2} \right] \right|. \quad (3)$$

By the Fourier transform of the nucleon current density, the nucleon current $J^\mu$ is written as

$$J^\mu = \int \bar{\psi}_p \hat{\mathbf{J}}^\mu \psi_b e^{i\mathbf{q}\cdot\mathbf{r}} d^3 r, \quad (4)$$

where $\hat{\mathbf{J}}^\mu$ is a free electroweak nucleon current operator, and $\psi_p$ and $\psi_b$ are wave functions of the knocked-out and the bound state nucleons, respectively. The wave functions are generated with the same models as the previous works [42,43]. For a free nucleon, the current operator of the CC reaction is composed of the weak vector and the axial vector form factors:

$$\hat{\mathbf{J}}^\mu = F_1^V(Q^2)\gamma^\mu + F_2^V(Q^2)\frac{i}{2M_N}\sigma^{\mu\nu}q_\nu + G_A(Q^2)\gamma^\mu\gamma^5 + \frac{1}{2M_N} G_P(Q^2) q^\mu \gamma^5. \quad (5)$$

By the conservation of the vector current (CVC) hypothesis, the vector form factors for the proton (neutron), $F_i^{V,\,p(n)}(Q^2)$, are expressed as

$$F_i^{V,p(n)}(Q^2) = F_i^p(Q^2) - F_i^n(Q^2). \quad (6)$$

The axial form factors for the CC reaction are given by

$$G_A(Q^2) = \frac{-g_A}{\left(1 + Q^2/M_A^2\right)^2} \quad (7)$$

with $g_A = 1.262$ and the global value of the axial mass is $M_A = 1.032$ GeV.

The induced pseudoscalar form factor is parametrized by the Goldberger-Treimann relation

$$G_P(Q^2) = \frac{2M_N}{Q^2 + m_\pi^2} G_A(Q^2), \quad (8)$$

where $m_\pi$ is the pion mass.

## III. RESULT

By using the QHD, NL, QMC, and CQMC nuclear models, we calculate various differential cross sections and total cross section in the quasielastic $(\nu_\mu, \mu^-)$ and $(\bar{\nu}_\mu, \mu^+)$ reactions off $^{12}$C and $^{40}$Ar, and compare the theoretical results with MiniBooNE, SciBooNE, T2K, and MicroBooNE data. In the neutrino experiments, the energy of incoming neutrino cannot be fixed, so the cross sections have to be averaged over the flux of the incident neutrino beam. In the previous work [30], we calculated the quasielastic $\nu$-$A$ scattering by varying the value of $M_A$ from the standard value to 1.39 GeV with the QHD model. But it was not enough to describe the MiniBooNE data even with 1.39 GeV because of excluding additional nuclear effect such as multinucleon emission. Hence, we just choose the standard value of $M_A$ in the present calculation. Note that the whole cross sections are divided by the number of nucleons which are involved in the reaction.

Figure 1 shows the flux-averaged double-differential cross sections in terms of three-momentum of outgoing muon at fixed polar angle of the muon. The solid (red), dashed (black), dotted (blue), and dash-dotted (sky blue) curves are the results of the QHD, NL, QMC, and CQMC models. Here, $^{40}$Ar is used as target nucleus and the experimental data were measured from MicroBooNE [14]. In this experiment, the momentum of the outgoing muon was measured by using multiple Coulomb scattering for the muon tracking in the detector and the data include $0\pi NP$ interaction channel meaning no pion with at least one proton ($N \geqslant 1$) in the final state. The red lines shift toward lower momentum relative to the others whose peaks are located almost at the same position. The magnitude of the CQMC is the smallest, which is suppressed by the quark-quark hyperfine interactions due to exchanges of gluon and pion. The effect of nonlinear $\sigma$ field decreases with larger angles although the peak of the NL approaches that of the QHD. The theoretical results at backward angles overestimate the data as in Fig. 1(a), shift toward large momentum around 90°, but describe the data relatively well at forward angle. Since the three-momentum transfer $q$ is large at backward angle, there are much room for not only pure quasielastic scattering but other processes like multinucleon interaction to be involved. Note that the central values for the $\cos\theta_\mu$ are used up to Fig. 4.

In Fig. 2, the flux-averaged double-differential cross sections are shown in terms of the polar angle of muon from $^{12}$C at fixed kinetic energy (central values) of the muon and the data were measured from MiniBooNE [2]. We took the experimental data from Table VI in Ref. [2] whose total normalized uncertainty is 10.7%. The unit of the kinetic energy $T_\mu$ for the outgoing muon is GeV. The explanation of the curves is the same as that of Fig. 1. On the left panel, our results do not agree with the data at low kinetic energy [Fig. 2(a)] because

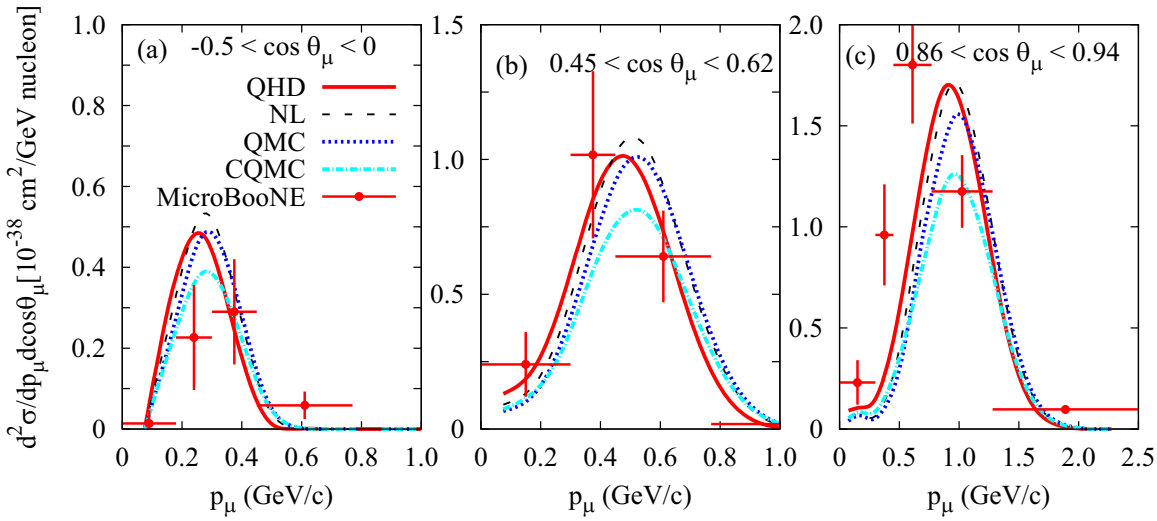


FIG. 1. Flux-averaged double-differential cross sections in terms of three-momentum of the outgoing muon from $^{40}$Ar. The data were measured by the MicroBooNE Collaboration [14].

of plausible multinucleon interactions but the agreement becomes much better at high kinetic energy [Fig. 2(b)]. In the latter case, the differences between the NL, QMC, and CQMC models are very tiny but the deviation of the QHD is large and even the peak shifts to right side. For this case, the effects of the nonlinear $\sigma$ field and the internal quark structure in a nucleon enhance the cross sections over the whole region of $T_\mu$ and shift toward lower $\cos\theta_\mu$.

As shown in Fig. 3, the flux-averaged double-differential cross sections off $^{12}$C are calculated with respect to the kinetic energy of the muon at fixed polar angle and the data were measured from MiniBooNE [2]. The peaks of theoretical results shift toward lower kinetic energy, and the magnitudes are underestimated by small amount on the left panel but on the right panel are overestimated except the red line. Like the previous case in Fig. 2, the results of the QHD are the smallest and the influence of quarks inside a nucleus appears clearly in the QMC and CQMC. On the left panel the effect of the nonlinear $\sigma$ field is very small. According to the results of Figs. 2 and 3, the role of internal quark structure enhances the double-differential cross sections and the effect of the nonlinear $\sigma$ field also increases the cross section except small $\cos\theta_\mu$.

In Fig. 4, we calculate the flux-averaged double-differential cross sections off $^{12}$C in terms of the momentum of muon at fixed polar angle and compare them with the data measured from T2K [12]. In this case, the kinematics are the same as the Fig. 1. In particular, the experimental data were measured without correcting for events where a pion is produced and we took the data for true $p_\mu$ and true $\cos\theta_\mu$ in Fig. 12 of Ref. [12]. Our theoretical cross sections describe the data very well even including the positions of the peaks compared with the MicroBooNE and MiniBooNE data. The magnitudes are relatively comparable in the theoretical results. In the case of this kinematics, the chiral effect from quark-quark interaction is the largest and the results of the NL and CQMC models are very close. These results are contrary to those of Fig. 1. The difference between two results is only target nucleus, that means, the influence of the quark-quark hyperfine interactions enhances the cross sections on $^{12}$C but reduces them on $^{40}$Ar.

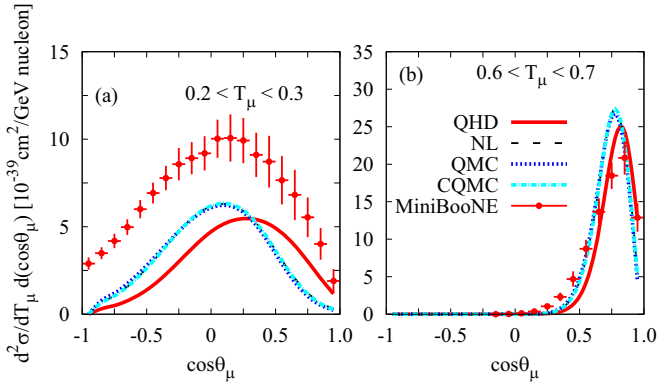


FIG. 2. Flux-averaged double-differential cross sections in terms of the scattering angle of the outgoing muon from $^{12}$C. The data were measured by the MiniBooNE Collaboration [2].

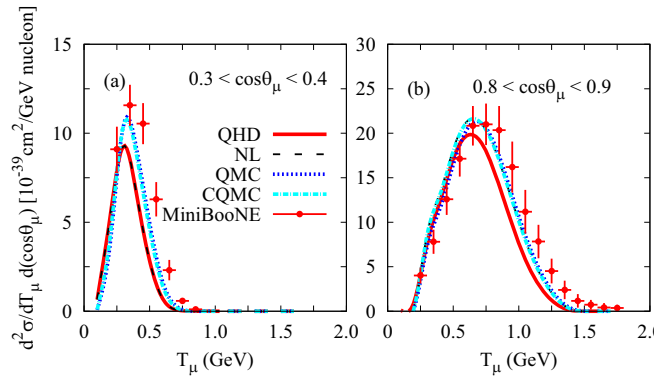


FIG. 3. Flux-averaged double-differential cross sections in terms of the kinetic energy of the outgoing muon from $^{12}$C. The data were measured by the MiniBooNE Collaboration [2].

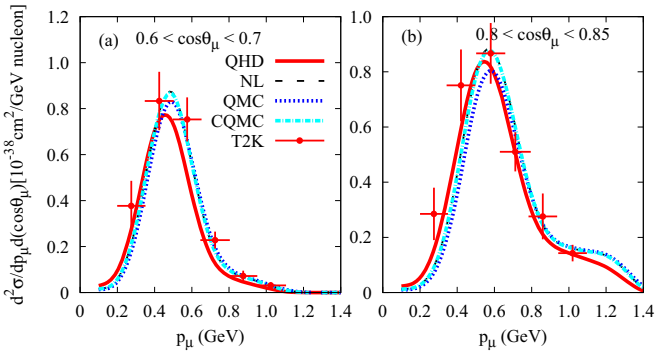


FIG. 4. Flux-averaged double-differential cross sections in terms of the three-momentum of the outgoing muon from $^{12}$C. The data were measured by the T2K Collaboration [12].

Figure 5 shows the flux-averaged single-differential cross sections off $^{40}$Ar in terms of total energy of the outgoing muon which are compared with the data from MicroBooNE [15]. This kinematics are similar to those of Fig. 1 due to the relation of $E_\mu = \sqrt{p_\mu^2 + m_\mu^2}$ after integrating the polar angle of the outgoing muon. While our theoretical results do not describe the data in Fig. 1, they are comparable with the data owing to the integration of the polar angle. The cross section of the CQMC is decreased by the hyperfine interactions and the nonlinear $\sigma$ field enhances the cross section like the previous one in Fig. 1. The peak of the QHD shifts to the lower $E_\mu$ about 100 MeV and the others are almost the same position with the data.

Figure 6 shows the flux-averaged single-differential cross section off $^{40}$Ar in terms of the energy transfer and we compare the cross section with the data measured from MicroBooNE [15]. The theoretical results do not describe the data at all for both the magnitude and the position of the peak. Figures 5 and 6 look quite different even though the cross sections are given separately by simple kinematical variables, the one by the muon energy $E_\mu$ and the other by the energy transfer $\omega$, that are related through $\omega = E_\nu - E_\mu$. This is basically

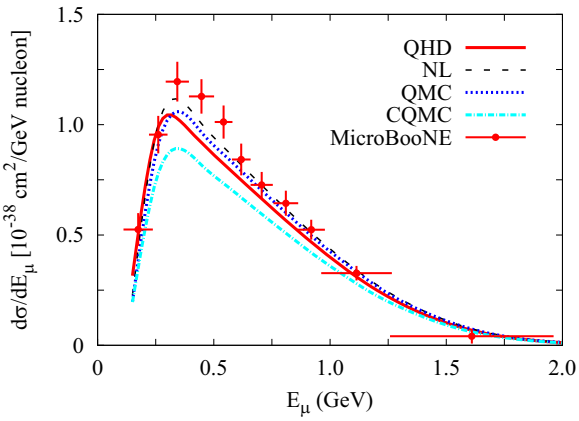


FIG. 5. Flux-averaged single-differential cross sections in terms of the outgoing muon energy from $^{40}$Ar. The data were measured by the MicroBooNE Collaboration [15].

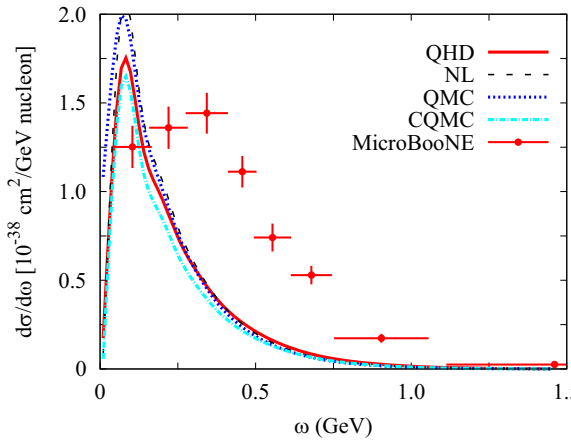


FIG. 6. Flux-averaged single-differential cross sections in terms of the energy transfer from $^{40}$Ar. The data were measured by the MicroBooNE Collaboration [15].

due to the fact that the incident neutrino beams are not monoenergetic and their flux averaging has to be adopted [14,15]. According to Ref. [47], $d\sigma/d\omega$ is advantageous as the various different reaction channels are entangled. But our results in Fig. 6 overestimate the MicroBooNE data only at lower $\omega$ and underestimate in the rest regions. Nevertheless, for the magnitude and the position of peak, our results are similar to Fig. 6 of Ref. [47]. In order to explain the MicroBooNE data, it may be necessary to include excited states generated by the RPA at lower $\omega$ and at higher $\omega$ to consider other inelastic processes like pion production. The quark-quark hyperfine interactions reduce the cross section and the nonlinear $\sigma$ field increases it like the previous results of Figs. 1 and 5.

In Fig. 7, the scaled total cross sections are shown in terms of the incident neutrino energy and are compared with MiniBooNE [2], SciBooNE [7], and MicroBooNE [15] data. The left panel is the results for the incident neutrino and the right panel is the results for the incident antineutrino. The scaled total cross section represents the total cross section divided by the number of nucleons which participate in the reaction. Although the theoretical results describe the MiniBooNE data for the case of the antineutrino, they do not describe the

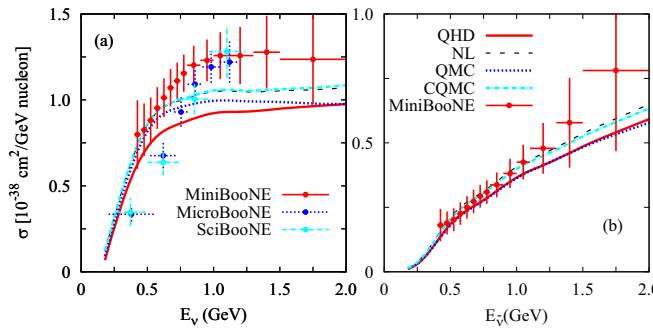


FIG. 7. Scaled total cross sections in terms of the incident neutrino energy (left) and the antineutrino energy (right). The data were measured by the MiniBooNE [2], SciBooNE [7], and MicroBooNE Collaboration [15].

data for the neutrino. Below 1 GeV, our results overestimate the SciBooNE and MicroBooNE data but underestimate the MiniBooNE data. Surprisingly, the experimental data do not agree with each other below 1 GeV. MiniBooNE data are much larger than the data from the other two experiments, SciBooNE and MicroBooNE. Note that the data measured from SciBooNE are inclusive by including a pion production, coherent pion production, and deep inelastic scattering.

## IV. SUMMARY

In the present work, we calculate the CC quasielastic scattering of the neutrino and antineutrino with $^{12}$C and $^{40}$Ar with four relativistic nuclear models and compare the theoretical results with MiniBooNE, SciBooNE, T2K, and MicroBooNE data. Both the wave functions of bound nucleon and outgoing nucleons are generated with the same nuclear potentials obtained from these models to include the final state interaction. Note that there are no any parameters to satisfy the experimental data except global values like an axial mass in the electroweak operator and we exclude the inelastic processes like MEC.

The double-differential cross sections in the CQMC model are the smallest in magnitude with respect to the momentum of the muon while in other cases those from the QHD model are the smallest. The theoretical cross sections describe properly the data from T2K but do not the data from MiniBooNE and MicroBooNE. The single-differential cross sections are calculated in terms of the muon energy and the energy transfer and compared with the data measured from MicroBooNE. The theoretical single-differential cross section for the muon energy describes the MicroBooNE data well but it elucidates the data no longer in terms of the energy transfer. The effect of the quark-quark hyperfine interactions due to exchanges of gluon and pion based on the chiral symmetry enhances the cross section on $^{12}$C but reduces it on $^{40}$Ar. The nonlinear $\sigma$ field enhances the cross section on both $^{12}$C and $^{40}$Ar. Finally, the scaled total cross sections are calculated with respect to the incident neutrino energy, and do not describe the data for the incident neutrino. But for the antineutrino case, they fit well with the MiniBooNE data.

In conclusion, the difference among four relativistic nuclear models (QHD, NL, QMC, and CQMC) is sensitive to kinematics and the cross sections generated from the models furnish the data relatively well. In particular, the different quark-quark interaction in the target may be an intriguing subject for the relativistic nuclear model. It is needed to figure out the difference between the MiniBooNE and SciBooNE (MicroBooNE) data, that means, more accurate experiment may be needed. It is also necessary to improve the nuclear model or to include the other process like multinucleon contribution to describe the experimental data precisely.

## ACKNOWLEDGMENTS

This work was supported by the National Research Foundation of Korea (NRF) grants funded by the Korea government (Nos. 2018R1A5A1025563, NRF-2018R1A2B6002432, NRF-2021R1F1A1046575, NRF-2021R1A6A1A03043957, NRF-2020K1A3A7A09080134, NRF-2020R1A2C3006177, and IBS-R031-D1) .

[1] V. Lyubushkin *et al.* (NOMAD Collaboration), Eur. Phys. J. C **63**, 355 (2009).
[2] A. A. Aguilar-Arevalo *et al.* (MiniBooNE Collaboration), Phys. Rev. D **81**, 092005 (2010).
[3] A. A. Aguilar-Arevalo *et al.* (MiniBooNE Collaboration), Phys. Rev. D **82**, 092005 (2010).
[4] A. A. Aguilar-Arevalo *et al.* (MiniBooNE Collaboration), Phys. Rev. D **88**, 032001 (2013).
[5] A. A. Aguilar-Arevalo *et al.* (MiniBooNE Collaboration), Phys. Rev. D **91**, 012004 (2015).
[6] A. A. Aguilar-Arevalo *et al.* (MiniBooNE Collaboration), Phys. Rev. Lett. **120**, 141802 (2018).
[7] Y. Nakajima *et al.* (SciBooNe Collaboration), Phys. Rev. D **83**, 012005 (2011).
[8] K. B. M. Mahn *et al.* (MiniBooNE and SciBooNE Collaborations), Phys. Rev. D **85**, 032007 (2012); G. Cheng *et al.* (MiniBooNE and SciBooNE Collaborations), *ibid.* **86**, 052009 (2012).
[9] L. Fields *et al.* (MINER$\nu$A Collaboration), Phys. Rev. Lett. **111**, 022501 (2013); G. A. Fiorentini *et al.* (MINER$\nu$A Collaboration), *ibid.* **111**, 022502 (2013).
[10] P. Adamson *et al.* (MINOS Collaboration), Phys. Rev. D **91**, 012005 (2015).
[11] K. Abe *et al.* (T2K Collaboration), Phys. Rev. D **92**, 112003 (2015); **98**, 032003 (2018).
[12] K. Abe *et al.* (T2K Collaboration), Phys. Rev. D **93**, 112012 (2016).
[13] P. Adamson *et al.* (NOvA Collaboration), Phys. Rev. Lett. **116**, 151806 (2016).
[14] P. Abratenko *et al.* (MicroBooNE Collaboration), Phys. Rev. Lett. **123**, 131801 (2019); **125**, 201803 (2020); Phys. Rev. D **102**, 112013 (2020).
[15] P. Abratenko *et al.* (MicroBooNE Collaboration), Phys. Rev. Lett. **128**, 151801 (2022).
[16] K. S. Kim, M.-K. Cheoun, and B. G. Yu, Phys. Rev. C **77**, 054604 (2008); K. S. Kim, H. Kim, M.-K. Cheoun, and W. Y. So, *ibid.* **94**, 064619 (2016).
[17] K. M. Graczyk and J. T. Sobczyk, Eur. Phys. J. C **31**, 177 (2003).
[18] N. Auerbach, N. Van Giai, and O. K. Vorov, Phys. Rev. C **56**, R2368 (1997).
[19] R. Perez, A. Deppman, A. R. Samana, E. Andrade-II, F. G. Velasco, and F. Guzman, Phys. Rev. D **105**, 063016 (2022).
[20] M. Martini, M. Ericson, and G. Chanfray, Phys. Rev. D **85**, 093012 (2012).
[21] A. Nikolakopoulos, M. Martini, M. Ericson, N. Van Dessel, R. Gonzalez-Jimenez, and N. Jachowicz, Phys. Rev. C **98**, 054603 (2018).
[22] A. Nikolakopoulos, V. Pandey, J. Spitz, and N. Jachowicz, Phys. Rev. C **103**, 064603 (2021).

[23] I. D. Kakorin, K. S. Kuzmin, and V. A. Naumov, Eur. Phys. J. C **81**, 1142 (2021).
[24] A. V. Butkevich and D. Perevalov, Phys. Rev. C **84**, 015501 (2011); Phys. Rev. D **89**, 053014 (2014); **99**, 093001 (2019).
[25] A. V. Butkevich, Phys. Rev. C **105**, 025501 (2022).
[26] M. Martini, M. Ericson, G. Chanfray, and J. Marteau, Phys. Rev. C **80**, 065501 (2009); M. Martini, M. Ericson, and G. Chanfray, *ibid.* **84**, 055502 (2011).
[27] J. Nieves, I. R. Simo, and M. J. Vicente Vacas, Phys. Rev. C **83**, 045501 (2011); J. Nieves, I. R. Simo, and M. J. Vicente Vacas, J. Phys.: Conf. Ser. **408**, 012040 (2013).
[28] J. E. Amaro and E. Ruiz Arriola, Phys. Rev. D **93**, 053002 (2016).
[29] G. D. Megias, J. E. Amaro, M. B. Barbaro, J. A. Caballero, T. W. Donnelly, and I. R. Simo, Phys. Rev. D **94**, 093004 (2016).
[30] K. S. Kim, K.-S. Choi, M.-K. Cheoun, W. Y. So, and H. Moon, Phys. Rev. C **100**, 034604 (2019).
[31] J. E. Sobczyk, J. Nieves, and F. Sanchez, Phys. Rev. C **102**, 024601 (2020).
[32] K. S. Kim, H. Gil, and C. H. Hyun, Phys. Lett. B **833**, 137273 (2022).
[33] J. D. Walecka, Ann. Phys. (NY) **83**, 491 (1974).
[34] C. J. Horowitz and B. D. Serot, Nucl. Phys. A **368**, 503 (1981).
[35] J. Boguta and A. R. Bodmer, Nucl. Phys. A **292**, 413 (1977).
[36] A. Bouyssy, S. Marcos, and P. Van Thieu, Nucl. Phys. A **422**, 541 (1984).
[37] Y. K. Gambhir, P. Ring, and A. Thimet, Ann. Phys. (NY) **198**, 132 (1990).
[38] P. A. M. Guichon, Phys. Lett. B **200**, 235 (1988).
[39] K. Saito and A. W. Thomas, Phys. Lett. B **327**, 9 (1994); K. Saito, K. Tsushima, and A. W. Thomas, Nucl. Phys. A **609**, 339 (1996); Phys. Rev. C **55**, 2637 (1997).
[40] S. Nagai, T. Miyatsu, K. Saito, and K. Tsushima, Phys. Lett. B **666**, 239 (2008).
[41] T. Miyatsu, M. K. Cheoun, and K. Saito, Phys. Lett. B **709**, 242 (2012); Astrophys. J. **813**, 135 (2015).
[42] S. Choi, T. Miyatsu, Y. Kwon, K. Kim, M.-K. Cheoun, and K. Saito, Phys. Rev. C **104**, 014322 (2021).
[43] K. S. Kim, S. Choi, M.-K. Cheoun, and H. Kim, Phys. Rev. C **105**, 024606 (2022).
[44] K. S. Kim, M.-K. Cheoun, and W. Y. So, Phys. Rev. C **88**, 044615 (2013).
[45] R. Gonzalez-Jimenez, A. Nikolakopoulos, N. Jachowicz, and J. M. Udias, Phys. Rev. C **100**, 045501 (2019).
[46] K. S. Kim, L. E. Wright, Y. Jin, and D. W. Kosik, Phys. Rev. C **54**, 2515 (1996); K. S. Kim, L. E. Wright, and D. A. Resler, *ibid.* **64**, 044607 (2001); K. S. Kim and L. E. Wright, *ibid.* **60**, 067604 (1999); **72**, 064607 (2005).
[47] M. Martini, M. Ericson, and G. Chanfray, Phys. Rev. C **106**, 015503 (2022).